*Int. J. Electrochem. Sci.*, 6 **(2011)** 4967 - 4983

International Journal of
ELECTROCHEMICAL
SCIENCE
www.electrochemsci.org

# Quantum-Chemistry Based Studying of Rebar Passivation in Alkaline Concrete Environment

*Tongyan Pan[1,*], and Yang Lu[2]*

[1] Department of Civil Engineering, The Catholic University of America, Washington, DC 20064, USA
[*]E-mail: pan@cua.edu

[2] Virginia Polytechnic Institute and State University, Blacksburg, Virginia, 24060, USA

*Received:* 5 August 2011 / *Accepted:* 3 September 2011 / *Published:* 1 October 2011

A clear understanding of the mechanisms of passivation and depassivation of steel surface is critical to the effective control of rebar corrosion. The process of passivation involves oxidation of iron atoms in the typical concrete environment. Traditional electrochemical approach of interpreting steel corrosion follows the changes in voltage and current as a result of electrode reactions, therefore is incapable of depicting iron oxidation and the incurred structural change at the atomic scale. A research study was conducted recently to simulate the passivation process of steel using a Quantum Chemistry-based reactive force field. The initiation and growth of oxides were found to be highly dependent on the thermodynamics and availability of reactants. Three oxidation stages were identified until a high-density triplex structure was formed on iron surface, after which the oxidation of iron progressed at a significantly reduced speed. Results from this study will benefit improving the knowledge base and controlling of rebar corrosion.

**Keywords:** Rebar Passivation, Quantum Chemistry, Concrete, Atomistic Modeling

## 1. INTRODUCTION

Being a destructive process, steel corrosion has been a potent force that depletes the natural resource of iron and causes expensive infrastructure deterioration, leading to impaired living environment and social economy [1-5]. Steel corrosion is a complex process that includes an initial process of steel surface passivation when the bulk iron is introduced to oxidizing agents, followed by subsequent passivation and depassivation cycles in environments of varying oxidizing capabilities. Passivation is the process in which a multi-layer iron oxide film is formed on steel surface when the surface iron atoms are exposed to and react with oxygen, hydroxyls and/or water molecules from the working environment of steel; whereas depassivation refers to the process in which the active corrosion gets initiated as the passive film formed in preceding passivation process is damaged and the bulk iron becomes re-exposed to oxygen, hydroxyls and/or water molecules for the further oxidation. Such general processes of passivation and depassivation are essentially the same for the active corrosion of steels in nearly all applications. One phenomenal case of steel corrosion is the corrosion of reinforcing bars in concrete structures (rebars), of which the destructive effects usually include the loss of steel, cracking/spalling of concrete caused by accumulated corrosion products at anodic sites, and eventually the failure of structure [6-14].

Depending on the extent of iron oxidation, the iron oxide layer formed on steel surface could have different levels of thickness, from a few angstroms to some tens of nanometers [15]. Accordingly, the extent of iron oxidation or passivation of steel surface depends much on the time and external environment in which the steel surface is oxidized. The oxide film formed in passivation usually has a denser structure and higher chemical stability than bulk iron, therefore tends to mitigate further iron oxidation by preventing the direct contact between bulk iron and oxygen, hydroxyls and/or water molecules. Therefore, the multi-layer iron oxide film on steel surface is commonly referred to as the "protective layer" or "protective film" to reduce corrosion rate [16]. When the steel surface is passivated, the corrosion usually progresses at low rate (less than one micrometer a year) that causes only minor iron loss and structural damages, and can be controlled by routine maintenance.

Therefore, to activate steel corrosion, the steel surface must be depassivated. This in nature can be achieved by different mechanisms such as decrease in hydroxyl concentration or dissolved oxygen gas in water that would result in thin and vulnerable protective film, or damages by corrosive chemical species that depassivate steel surface by directly attacking the protective film. In a typical concrete environment (pH = 11.5~13.5), the rebar surface is exposed to the pore solution of concrete. Being more oxidizing for iron than water molecules, the hydroxyls can oxidize steel surface more easily and faster than water molecules, therefore facilitate the growth of a thicker protective film. The hydroxyl-driven passivation is the major mechanism for long-term corrosion resistance of steel in concrete [6, 7]. However, due to the instantaneous reaction time of initial iron oxidation and the significantly low percentage of hydroxyls relative to that of water molecules, hydroxyls may contribute little to the formation of the initial passivation. Accordingly, the very initial passivation of steel surface entails primarily the oxidation between iron atoms and water molecules (instead of hydroxyls) [16-18].

In the state-of-the-art of steel corrosion, there exist a series of fundamental issues that are not clearly understood in spite of the abundant knowledge developed in the science of electrochemistry. Among the fundamental issues, the atomic-level mechanism of iron oxidation and the growth pattern of oxidation products on steel surface are two well-known ones [16-20]. Without a clear understanding of these issues, the effective control of steel corrosion cannot be satisfactorily achieved. One direct consequence of missing a clear picture of these mechanisms is the lack of fundamental information in the formation and destruction of protective film on steel surface. Particularly related to rebar corrosion in concrete, such information is critical to the determination of the growth rate and pattern of corrosion products on steel surface, which in turn control the rate and pattern of concrete cracking/fracture (due to the expansion of the accumulated corrosion products at the steel-concrete interface). Within this context, a research study was recently launched to explore the atomic-scale mechanism of steel passivation and depassivation. This manuscript presents the results of studying the initial passivation phenomenon in a typical concrete environment.

### *1.1. Objectives*

There are three critical steps involved in the active corrosion of a rebar: (1) the initial oxidation of iron atoms at the anodes and reduction of hydrogen ions or oxygen molecules at the cathodic sites that involve electron transfer reactions, (2) passivation—subsequent formation of the protective oxide film that includes ferrous and ferric cations, oxygen atoms, and/or hydroxyls, and finally (3) depassivation—the destroy of the protective oxide film that relates to ferrous and ferric oxides, chloride anions. These three processes occur in the electric double layer at the steel-concrete interface, and are repeatable in an active corrosion. Central to the understanding of the steel corrosion, therefore, are the atomic-level structure change and dynamics of the oxidant/reductant atoms, ions and molecules in interaction with water molecules at the in the electric double layer. This paper focuses on modeling of two important processes involved in the Steps (1) and (2), i.e., the initial oxidation of iron atoms at the anodes and the formation of passive film on steel surface in a typical concrete environment.

### *1.2. Traditional Electrochemistry of Reinforcement Corrosion*

Steel corrosion reactions in concrete are electrochemical in essence [6-8]. The traditional kinetic approach of interpreting electrochemical phenomena follows voltage and current changes as a result of electrode reactions and ionic movement. From the perspective of classical electrochemistry, iron at anodic surface goes into pore solution of concrete as ferrous ions, which constitutes the anodic reaction. As iron atoms undergo oxidation, they release electrons that carry negative charge, which build up inside the steel and lead to a lower electric potential at the anodic sites. The anodic reaction continues as the electrons released pass to a different site (at a higher electric potential) on steel surface where the cathodic reaction occurs. At the cathodic site the extra electrons react with certain reducible components from the electrolyte and get removed off the steel.

Driven by the anodic reaction, the corresponding cathodic reaction will reach an equivalency state according to the Faraday's Laws as determined by the total flow of electrons from anodes to cathodes, i.e., the corrosion current, "$I_{cor}$". The corroding piece of steel is commonly described as a "mixed electrode" since the anodic and cathodic reactions proceed simultaneously on its surface. Accordingly, the electrochemical reactions in the corrosion of iron include Equations 1 and 2.

Anodic Reaction: $Fe \rightarrow Fe^{2+} + 2e$ (1)

Cathodic Reactions: $2H^{+} + 2e \rightarrow H_2$ (2a)

$$4H^{+} + O_2 + e^{-} \rightarrow H_2O \tag{2b}$$

$$H_2O + \frac{1}{2}O_2 + 2e \rightarrow 2OH^{-} \tag{2c}$$

Reaction per Equation 2a is common in a deaerated acid environment, while Equation 2b occurs in aerated, acid to neutral environments such as seawater and atmospheric weathering where oxygen is sufficiently available. In an electrolyte with pH > 8.5 and sufficient oxygen, the more important reaction is oxygen reduction per Equation 2c, in which corrosion is accompanied by the formation of solid corrosion debris from the reaction between the anodic and cathodic products (per Equation 3).

$$Fe^{2+} + 2OH^{-} \rightarrow Fe(OH)_2 \qquad (3)$$

The ferrous hydroxide produced by initial corrosion is subjected to further oxidation in the ambient condition. Even though the ferrous hydroxide is soluble (poorly though), most other iron oxides, hydroxides and oxy-hydroxides do not, such as the ferric hydroxide. These compounds, once formed in an aqueous solution (electrolyte), will deposit on steel surface. Such solid corrosion products deposited directly on the steel surface provide a protective surface film to retard further corrosion. The surface therefore becomes "passive", or "passivated". In the case of rebars, such a process is encouraged in the oxidizing environment of concrete and leads to the production of a film composed of oxides, hydroxides and oxy-hydroxides on steel per Equation 4. Equation 4 is not intended to give the exact formula of the corrosion products; instead it indicates the possibility of oxygen atom(s), hydroxyl(s), and water molecule(s) to bond with the iron ion(s) in the film of iron oxides, hydroxides and oxy-hydroxides. The symbols $n$, $m$, $x$, $y$, $z$ and $w$ each have a value ≥ 0.

$$Fe(OH)_2 + nO_2 + mH_2O \rightarrow Fe_xO_y(OH)_z \cdot (H_2O)_w \qquad (4)$$

However, in most service conditions, rebars are often subjected to corrosion (continued oxidation of bulk iron in steel) due to the access to aggressive chemical species including mainly chlorides, carbon dioxide, and sulfur oxides from the surrounding environment, especially the chlorides from road deicing application or marine environment. These species, can lower the pH level in concrete (by carbon dioxide or sulfur oxides) or destroy the protective passive film (by chlorides) when reaching steel surface, expose bulk steel to water and oxygen, and cause active corrosion of steel. The process of destroying the protective passive film is commonly referred to as "depassivation".

Further oxidation of the iron compounds in the right-hand side of Equation 4 eventually leads to red-colored products on the surface of steel—the "rust" that forms a mixture whose exact constitution depends also on other trace elements. It is the continued formation of the rust materials (in active corrosion) that leads to significant volumetric increase (up to 6.5 times of the volume of consumed iron) and causes destructive damage to the R/C structures.

### *1.3. Fundamentals of Reactive Force Field:*

Recent computing capacity has significantly improved the speed of modern quantum chemistry (QC) methods that enables predicting accurately the geometries, energies, and vibrational energies

(*21*). However, extensive use of QC methods today are still limited to small atomic systems or molecules, and is not yet practical for studying dynamic properties of larger systems. As such, it is necessary to have an accurate force field to quickly evaluate the inter-entity bonding, forces and other important dynamical properties such as the effects of deposition and diffusion of molecules (or other new products). Such an *ab initio (or first principles)*-based force field has the advantage of simulating chemical reactions while obtaining fast computation as traditional force fields do; therefore is highly desired for simulating iron oxidation that involves thousands of atom and molecules for a realistic simulation.

One QC-based force field force field is the reactive force field (ReaxFF) developed by van Duin et al. (*22*) that since advent has been parameterized and tested for a variety of materials and processes, including hydrocarbon reactions, transition-metal-catalyzed nanotube formation, and high-energy materials. Recently ReaxFF has been extended to more materials including various metals, ceramics, silicon, and polymers, and is now used as a general tool for chemical simulations.

The ReaxFF force field is a special type of force field that bridges the gap between computational quantum-chemistry method and the traditional molecular dynamics (MD) method. Computational quantum-chemistry methods, such as those based on the Density Functional Theory are limited in computation capacity, typically less than 100 atoms with today's computation capability, whereas traditional MD can handle thousands of atoms but is not capable of simulating chemical reactions (generation of chemical bonds such as metallic bonds, ionic bonds, covalence bonds, etc., therefore new chemical species). The traditional MD methods are based on classical mechanics such as the Newtonian Mechanics or Hamiltonian Mechanics, therefore can only simulate non-chemical interatomic forces such as the van der Waals and Coulomb forces like that in the classical Lennard-Jones model. Parameterized on computational quantum-chemistry, the ReaxFF force field is capable of simulating chemical reactions and handling thousands of atoms at a reasonable computation speed.

Moreover, since the ReaxFF force field is capable of simulating any possible chemical reactions among the three elements: iron, oxygen, hydrogen, the atomistic model developed in this study is applicable to any types of crystal surfaces that can be realistically formed in nature. Hence the atomistic model developed in this study is capable of qualitatively differentiating different crystal surfaces.

The overall energy of a ReaxFF system contains a series of partial energies or energy contributions per Equation 5, all determined based on QC. The actual number of partial energies of a system depends on the type of material and reactions to be modeled. More complex systems usually require more such partial energy terms. The ReaxFF for simulating oxidation of iron in the steel-water double-layer system involves complex chemical reactions between the iron, oxygen, hydrogen elements.

$$E_{system} = E_{bond} + E_{val} + E_{tors} + E_{vdWaals} + E_{Coulomb} \tag{5}$$

In Equation 5, the bond energy $E_{bond}$ describes the chemical energy between each pair of bonded atoms. Valence angle energy $E_{val}$ accounts for the energy contribution from valence angle; torsion rotation energy $E_{tors}$ ensures proper dependence of the energy of torsion angle for bond order approaching zero and bond order greater than 1; van der Waals interactions energy $E_{vdWaals}$ accounts for the van der Waals interactions; and Coulomb interactions energy $E_{Couloms}$ between all atom pairs adjust for orbital overlap between atoms at close distances.

The fundamental ReaxFF assumption is that the bond order $BO'_{ij}$ between a pair of atoms is dependent on the interatomic distance $r_{ij}$ according to Equation 6, in which the parameter $r_0$ is the bond radius and the series of parameters $p$s describe the bond order. In calculating bond orders, ReaxFF distinguishes between contributions from $\sigma$ bonds, $\pi$ bonds, and $\pi\pi$ bonds. The bond orders $BO'_{ij}$ are updated in each time step. The energy of the system is finally determined by summing up the partial energy contributions including the bond energy, valence angle energy, torsion angle energy, etc., and non-bonded van der Waals and Coulomb energies per Equation 5.

$$BO'_{ij} = BO^{\sigma}_{ij} + BO^{\pi}_{ij} + BO^{\pi\pi}_{ij} = \exp\left[p_{bo1} \cdot \left(\frac{r_{ij}}{r^{\sigma}_{o}}\right)^{p_{bo2}}\right] + \exp\left[p_{bo3} \cdot \left(\frac{r_{ij}}{r^{\pi}_{o}}\right)^{p_{bo4}}\right] + \exp\left[p_{bo5} \cdot \left(\frac{r_{ij}}{r^{\pi\pi}_{o}}\right)^{p_{bo6}}\right] \quad (6)$$

The three pairs of parameters: $p_{bo,1}$ and $p_{bo,2}$, $p_{bo,3}$ and $p_{bo,4}$, and $p_{bo,5}$ and $p_{bo,6}$ in Equation 6 correspond to the orders of the $\sigma$ bond, the first $\pi$ bond, and the second $\pi\pi$ bond, respectively. The values of the exponential terms is unity below a particular interatomic distance $r_0$ and negligible at a longer distance. The bond energy is calculated from the bond order $BO'_{ij}$. The following sections introduced these energy contribution terms.

### *1.4. Bond Energy*

$\boldsymbol{E_{bond}}$ is determined according to Equation 7. $D_e$ and $p_{be,1}$ and $p_{be,2}$ are bond parameters. Upon the dissociation of a bond, the bond order $BO'_{ij}$ approaches zero making the bond energy term $E_{bond}$ disappear. To simulate oxidation of iron, the partial energies developed by Aryanpour et al. (*23*) are used to determine the overall system energy—hence the ReaxFF potential function—for the atomic-level modeling of oxidation iron, with the parameters given in Table 1.

$$E_{bond} = -D^{\sigma}_{e} \cdot BO^{\sigma}_{ij} \cdot \exp[p_{be1}(1-(BO^{\sigma}_{ij})^{p_{be2}})] - D^{\pi}_{e} \cdot BO^{\pi}_{ij} - D^{\pi\pi}_{e} \cdot BO^{\pi\pi}_{ij} \quad (7)$$

**Table 1.** Parameters for the Determination of Bond Energy

| Bond | $D_e$ (kcal/mol) | $p_{be,1}$ | $p_{be,2}$ | $p_{bo,1}$ | $p_{bo,2}$ | $p_{bo,3}$ | $p_{bo,4}$ | $p_{bo,5}$ | $p_{bo,6}$ |
|---|---|---|---|---|---|---|---|---|---|
| Fe-H | 105.0054 | -0.0717 | 0.1000 | -0.1216 | 4.5062 | 1.0000 | 0.0000 | 0.0000 | 6.0000 |
| Fe-O | 65.7713 | 0.1366 | 0.9495 | -0.0555 | 7.9897 | -0.3500 | 15.0000 | -0.3000 | 36.0000 |
| Fe-Fe | 38.7471 | 0.3595 | 1.0000 | -0.0771 | 6.4477 | -0.2000 | 15.0000 | -0.2000 | 16.0000 |
| H-O | 160.0000 | -0.5725 | 1.1150 | -0.0920 | 4.2790 | 1.0000 | 0.0000 | 0.0000 | 6.0000 |
| H-H | 153.3934 | -0.4600 | 6.2500 | -0.0790 | 6.0552 | 1.0000 | 0.0000 | 0.0000 | 6.0000 |
| O-O | 142.2858 | 0.2506 | 0.3451 | -0.1225 | 5.5000 | -0.1055 | 9.0000 | -0.1000 | 29.7503 |

*1.5. Valence Angle Energy*

***$E_{val}$*** is computed according to Equation 8 that determines the energy associated with deviations in valence angle $\Theta_{ijk}$ from its equilibrium value $\Theta_0$. The term $f_1(BO)$ per Eq. 8a ensures that the valence angle energy contribution disappears smoothly during bond dissociation. Eq. 8b deals with the effects of over/under coordination in central atom $j$ on the valence angle energy. Atom undercoordination/overcoordination parameter $\Delta_j$ is defined for atoms as the difference between the total bond order around the atom and the number of its bonding electrons valence. Table 2 lists the values of parameters used to determine the valence angle energy $E_{val}$.

$$E_{val} = f_1(BO_{ij}) \cdot f_1(BO_{jk}) \cdot f_2(\Delta_j) \cdot \{p_{val1} - p_{val1} \exp[-p_{val2}\left(\Theta_o(BO) - \Theta_{ijk}\right)^2]\} \tag{8}$$

$$f_1(BO_{ij}) = 1 - \exp\left(-BO_{ij}^{p_{val3}}\right) \tag{8a}$$

$$f_2(\Delta_j) = \frac{2 + \exp(\Delta_j)}{1 + \exp(\Delta_j) + \exp(-p_{val4} \cdot \Delta_j)} \tag{8b}$$

**Table 2** Parameters for the Determination of Valence Angle Energy

| Angle | □$_0$ (deg) | $p_{val,1}$(kcal/mol) | $p_{val,2}$(1/radian$^2$) | $p_{val,3}$ | $p_{val,4}$ |
|---|---|---|---|---|---|
| O-Fe-H | 34.0653 | 20.1868 | 4.7461 | 1.6752 | 0.1000 |
| O-H-Fe | 0.0000 | 4.6026 | 2.5343 | 1.1051 | 0.7284 |
| O-Fe-Fe | 65.7545 | 5.6268 | 4.0645 | 2.6730 | 1.7794 |
| O-O-Fe | 73.6721 | 32.633 | 1.7223 | 1.4351 | 1.0221 |
| H-O-Fe | 59.4556 | 10.2025 | 0.7481 | 1.0000 | 1.4521 |
| Fe-O-Fe | 57.6787 | 4.8566 | 2.5768 | 1.0000 | 0.7552 |
| O-Fe-O | 79.7335 | 0.0100 | 0.1392 | 2.1948 | 0.4968 |
| H-Fe-Fe[1] | 180.0000 | -6.9970 | 24.3956 | 1.3672 | 0.7878 |
| H-Fe-Fe[2] | 21.2590 | 6.5954 | 0.9951 | 1.0000 | 2.8006 |
| Fe-H-Fe | 0.0000 | 8.2994 | 5.7832 | 1.7716 | 2.9873 |
| H-H-Fe | 0.1000 | 30.0000 | 3.4094 | 1.5166 | 2.4379 |
| H-Fe-H | 34.1965 | 6.6782 | 6.5943 | 1.5365 | 1.3895 |

*1.6. Torsion Rotation Energy*

***$E_{tors}$*** ensure that dependence of the energy of torsion angle $\omega_{ijk}$ accounts properly as bond order approaches zero and bond order greater than 1. This is given in Equations 9 and 9a-9b. $\Theta_{ijk}$ and $\Theta_{jkl}$ are valence angles. $\Delta$ is the atom undercoordination/overcoordination parameters. Parameters $p_{tor3}$ and $p_{tor4}$ in Equation 9b equal zero for the specific types of elements in this study. Table 3 lists the values of parameters $V_1$, $V_2$, $V_1$ and $p_{tor}$ used to determine the torsion rotation energy $E_{tors}$.

$$E_{tors} = f_3(BO_{ij}, BO_{jk}, BO_{kl}) \cdot \sin\Theta_{ijk} \cdot \sin\Theta_{jkl} \left[\frac{1}{2}V_2 \cdot \exp\left\{p_{tor} \cdot (BO_{jk} - 1 + f_4(\Delta_i, \Delta_k))^2\right\} \cdot (1 - 2\cos\omega_{ijkl}) + \frac{1}{2}V_3(1 + \cos 3\omega_{ijkl})\right] \quad (9)$$

$$f_3(BO_{ij}, BO_{jk}, BO_{kl}) = [1 - \exp(BO_{ij})] \cdot [1 - \exp(BO_{jk})] \cdot [1 - \exp(BO_{kl})] \quad (9a)$$

$$f_4(\Delta_j, \Delta_k) = \frac{2 + \exp(-\Delta_j - \Delta_k)}{1 + \exp(-\Delta_j - \Delta_k) + \exp(\Delta_j + \Delta_k)} \quad (9b)$$

**Table 3** Parameters for the Determination of Torsion Rotation Energy

| Torsion Angle | $V_1$(kcal/mol) | $V_2$ (kcal/mol) | $V_3$ (kcal/mol) | $p_{tor}$ |
|---|---|---|---|---|
| O-O-O-O | -2.5000 | -25.0000 | 1.0000 | -2.5000 |
| H-O-O-O | -2.5000 | -2.5103 | -1.0000 | -2.5000 |
| H-O-O-H | 2.5000 | -22.9397 | 0.6991 | -3.3961 |

*1.7. Van der Waals Interactions Energy*

***E**$_{vdWaals}$* accounts for the van der Waals interactions using a distance-corrected Morse-potential given in Equation 10. By including a shielded interaction (Eq. 10(a)), excessively high repulsions between bonded atoms (1-2 interactions) and atoms sharing a valence angle (1-3 interactions) are avoided. $D_{ij}$ is the basic energy term of an atomic pair; $r_{vdW}$ is the van der Waal radius. The parameter $\alpha_{ij}$ is set to be 1 for the elements of this study. The other parameters for $E_{vdWaals}$ are given in Table 4.

$$E_{vdWaals} = D_{ij} \cdot \left\{\exp\left[\alpha_{ij} \cdot \left(1 - \frac{f_{13}(r_{ij})}{r_{vdW}}\right)\right] - 2 \cdot \exp\left[\frac{1}{2} \cdot \alpha_{ij} \cdot \left(1 - \frac{f_{13}(r_{ij})}{r_{vdW}}\right)\right]\right\} \quad (10)$$

$$f_6(r_{ij}) = \left[r_{ij}^{p_{vdW1}} + \left(\frac{1}{\gamma_w}\right)^{p_{vdW1}}\right]^{\frac{1}{p_{vdW1}}} \quad (10a)$$

**Table 4** Parameters for the Determination of van der Waals Interaction Energy

| Atom Pair | $D_{ij}$ (kcal/mol) | $r_{vdW}$ (Å) | $\square_w$ | $p_{vdW1}$ |
|---|---|---|---|---|
| Fe-H | 0.0640 | 1.6974 | 11.5167 | -1.0000 |
| Fe-O | 0.0846 | 1.4284 | 10.0808 | -1.0000 |
| H-O | 0.0283 | 1.2885 | 10.9190 | -1.0000 |

### *1.8. Coulomb Interactions Energy*

$\boldsymbol{E_{Couloms}}$ is considered between all atom pairs. To adjust for orbital overlap between atoms at close distances a shielded Coulomb potential $E_{Couloms}$ is used (see Equation 11).

$$E_{Coulcomb} = C \cdot \frac{q_i \cdot q_j}{\left[ r_{ij}^3 + \left(1/\gamma_{ij}\right)^3 \right]^{1/3}} \tag{11}$$

Atomic charges are calculated using the electron equilibration method (*24*, *25*). The initial values for the electron equilibration method parameters ($\eta$, $\chi$, and $\gamma$) were determined by Njo et al. (*26*). The optimization parameter $\gamma_{ij}$ in Eq. 11 is included for orbital overlap correction in the electron equilibration method.

### *1.9. Atomistic Modeling of Iron Oxidation*

Steel is compositionally an alloy of iron, carbon and some trace metals including mainly the chromium, cobalt, columbium, molybdenum, nickel, titanium, tungsten, vanadium and/or zirconium. Iron is the primary ingredient in general structural steels. At normal temperatures (< 912°C), bulk-iron metal is well-known to be α-iron, also known as ferrite that has the stable crystalline structure of body-centered cubic (bcc). The bcc structure has a relatively low packing density of the bulk structure, of which the surfaces tend to be of a rather open nature with surface atoms often exhibiting rather low coordination numbers.

The bcc structure has three surfaces, i.e., the (100), (110), and (111) in terms of Miller Indices, of which the (100) surface is obtained by cutting the metal parallel to the front surface of the bcc cubic unit cell - to expose a relatively open surface with an atomic arrangement of 4-fold symmetry. The (110) surface is obtained by cutting the metal in a manner that intersects the x and y axes but creates a surface parallel to the z-axis - to expose a surface which has a higher atom density than the (100) surface. The (111) surface of the bcc structure has a surface atomic arrangement that exhibits 3-fold; it is a much more open surface with atoms in both the second and third layers clearly visible when the surface is viewed from above. In this study, the (100) surface is modeled to investigate the most stable surface of iron (with the least surface atom exposure of the three types of surfaces). The carbon and the trace metals are not modeled due to their scarcity to appear in a typical atomic-scale domain.

To study the oxidation of reinforcing steels in their service conditions, the condition of a typical ambient environment is simulated—at an intermediate temperature (25°C) and under one standard atmospheric pressure (1 ATM). To build the ReaxFF model, 900 Fe atoms forming a thin piece of iron sheet (with two (100) bcc surfaces and a thickness of nine iron atoms) are included in a bulk water domain to simulate the water film in the ambient condition (see Fig. 1). The bcc crystalline structure of iron has a lattice constant $a$ = 2.87Å. The inter-molecule distance between water molecules is determined based on the density of water at the temperature of 25°C and under 1 ATM, which equals 997.05 kg/m$^3$. The bulk water is simulated to have pH of 12.5.

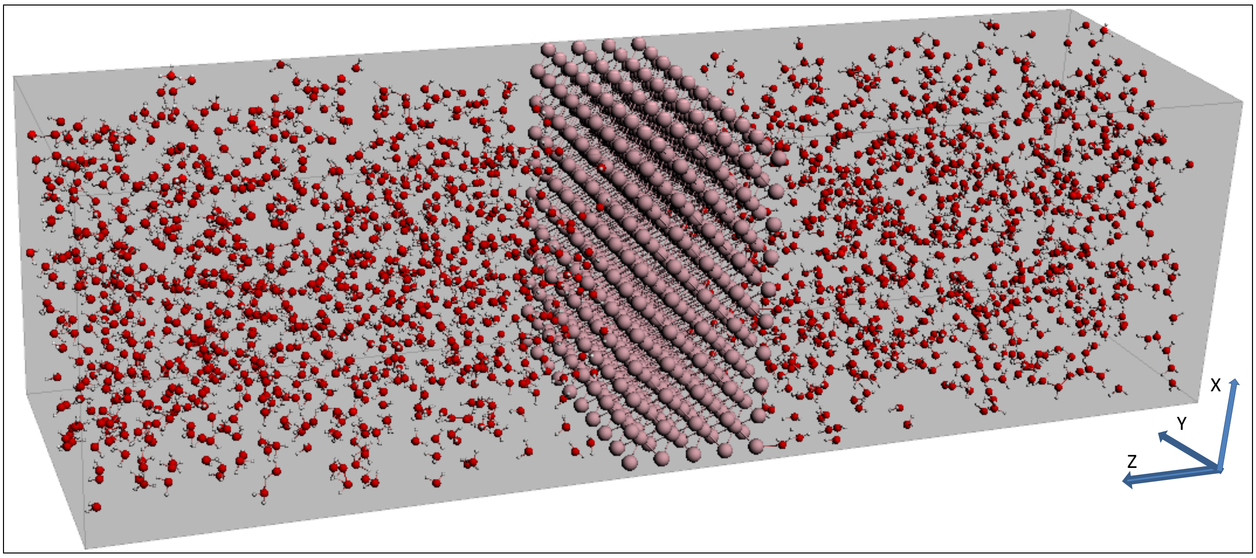


**Figure 1.** ReaxFF Model of Iron Oxidation

The ReaxFF model has the dimensions of X = 28.7 Å, Y = 28.7 Å, and Z = 100 Å that contains a total of 2,300 water molecules and four hydroxyls ($OH^-$) to simulate the condition of pH = 12.5. At pH = 12.5, ReaxFF also generates approximately $5\times10^{-6}$ $H^+$ and $OH^-$ ions in the modeled domain, which are significantly less than one and can only be witnessed momentarily. The ReaxFF model was run at a Velocity Verlet plus Berendsen ensemble at a time step of 0.25 femtoseconds (fs). The iron oxidation model was run using a parallel computing algorithm developed based on the MPI (Message-Passing Interface) Standard. The Virginia Tech's suite of high performance computers—System X, a supercomputer comprising 1,100 Apple PowerMac G5 cluster nodes was used for the computation. System X is capable of running at 12.25 Teraflops (meaning $10^{12}$ FLoating point OPerations per Second). The ReaxFF model is run until iron atoms are completely oxidized/hydroxidized/oxy-hydroxidized when the crystalline structure of the bulk iron will also be destructed.

## 2. RESULTS AND DISCUSSIONS

The primary goal of this study is to observe the types and amount of the generated chemical species including iron hydrates, oxides, hydroxides or oxy-hydroxides produced on steel surface. Throughout the simulation period, the process of chemical reactions was studied by monitoring the generation of new chemical species, mainly the types and amount of Fe—O bond formed in the iron oxidation process. Equally importantly in the iron oxidation process are morphological and crystalline structural changes occurring to the bulk materials (originally bulk iron and subsequently bulk hydrates/oxides/hydroxides/ oxy-hydroxides). Based on the types and amount of generated Fe—O bond and the changes in the crystalline structure and morphology of bulk materials, the oxidation process of iron is divided in three stages:

**Stage I:** Hydration of first-layer iron atoms—the products of this stage are the hydrates of iron atoms, i.e., $H_2O \cdot n$Fe, on the very surface layer of bulk metal, with *n* observed to vary between 0 – 3. As shown in Fig. 2(a), the Fe atom(s) is bonded with the oxygen atoms from water molecules. It is noteworthy that not every top-layer Fe atom gets immediately bonded with oxygen atoms (n = 0); however, as time goes, more and more surface Fe atoms become bonded. The bulk metal surface therefore becomes "saturated" with water molecules. In this stage, there are no obvious changes demonstrated in the crystalline structure, volume, density and morphology of the bulk iron, which indicates that the $H_2O$—Fe bonds formed in the hydration stage are weaker than the metallic bond between Fe atoms in bulk iron.

The newly generated Fe-$H_2O$ hydrates throughout the first stage (before the de-bonding of the first proton from water molecule) are recorded as shown in Fig. 2(b). Stage I is an instantaneous process in the ambient condition that takes about 3000 iterations (equal to 0.75 picoseconds). Of the 16 types of oxides/hydroxides/oxy-hydroxides ever observed on the planet of earth, none of them were generated in this stage, which means that the observed intermediate oxidation products and chemically unstable.

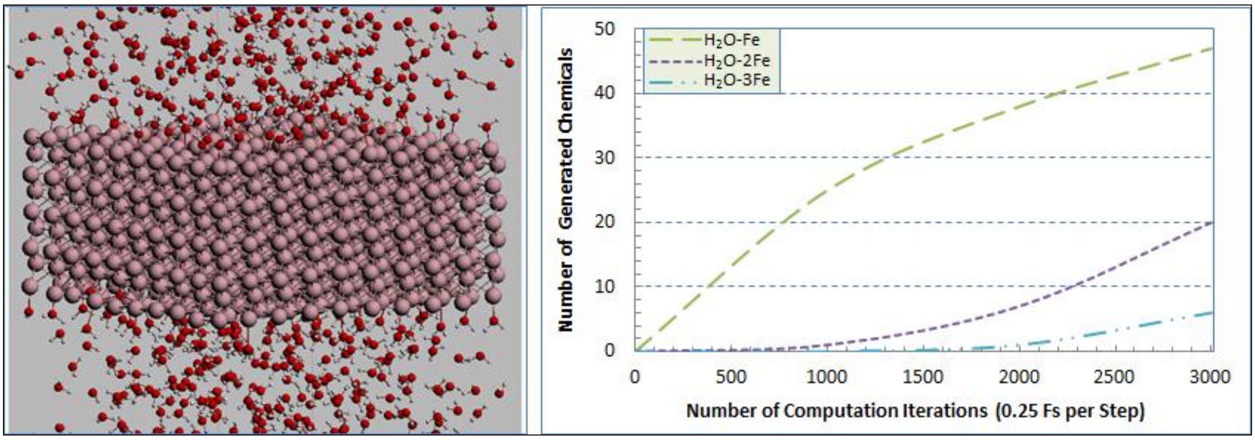


**Figure 2.** (a) Hydration of Iron in Stage I; (b) Generation of New Chemicals in Stage I

**Stage II:** Oxidation/hydroxidation of top iron layers—as the running time progresses further, de-bonding of hydrogen atoms (protons) occurs (from oxygen atom) in some water molecules that were originally bonded with two or three Fe atoms, which immediately results in the generation of $H^+$ cations or hydrogen gas molecules. The oxygen atoms, after losing one or two protons, become more strongly bonded with the surface Fe atoms. With a smaller size than water molecule, these oxygen atoms and hydroxyls however are subjected to the influence of inner-layer Fe atoms and some of them tend to enter the bulk iron from the gap space between the top-layer iron atoms. The attraction seemed to come mainly from the second-layer Fe atom located right below the top-layer inter-atom gap. These few oxygen atoms or hydroxyls gradually form chemical bond(s) with the second-layer Fe atoms.

Similarly, influential force was executed to the oxygen atoms bonded to the second-layer Fe atoms by the third- or deeper layer(s) Fe atoms. Some oxygen atoms move further into the bulk iron and get bonded with the third-layer Fe atoms. Although it is possible that hydroxyls also form bond with the third-layer Fe atoms, this phenomenon was not observed throughout the simulation process. Fig. 3(a) shows the oxidation of Fe atoms under the surface layer of bulk iron through this mechanism. Phenomenologically, the deeper into the bulk iron, the less oxygen atoms there are available to oxidize Fe atoms.

As more oxygen atoms become bonded with the inner-layer Fe atoms, water molecules from bulk water continue getting bonded with the top-layer Fe atoms, leading to the top of iron "saturated" with water molecules and, to a much less extent, some oxygen atoms and hydroxyls. The snapshot in Fig. 3(a) shows the top three layers of Fe atoms bonded with a collection of water molecules, hydroxyls and oxygen atoms, with primarily water molecules and hydroxyls bonded with the surface-layer Fe atoms and oxygen with the second and third layer Fe atoms. The concurrent hydration, oxidation, hydroxidation and oxy-hydroxidation processes occurring to the top-layer iron atoms constitute a representative picture of the Stage II reactions under a typical ambient condition. Fig. 3(a) shows obvious dis-location of Fe atoms started in the surface two layers and the corners (from their original crystalline locations).

The new chemical species generated in Stage II (before all the metallic bonds of the first Fe atom break from bulk iron) are recorded in Fig. 3(b). Stage II takes about $3.0\times10^{9}$ iterations, or 0.75 microseconds to complete in the ambient condition, which is significantly longer time than Stage I. One characteristic feature of Stage II is that none of the Fe atoms (HO-Fe, HO-2Fe, HO-3Fe, O-Fe, O-2Fe, and O-3Fe) in bond with oxygen atoms are fully oxidized to their highest valence number, +3 for Fe).

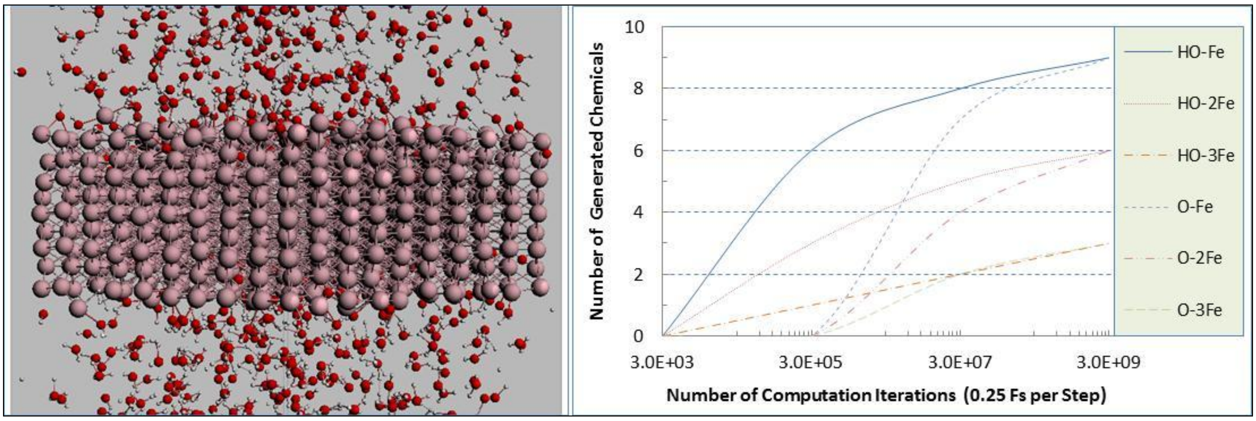


**Figure 3.** (a) Oxidation of Iron in Stage II; (b) Generation of New Chemicals in Stage II

Although the original oxidization of inner-layer Fe atoms by a few oxygen atoms does not cause significant change in the crystalline structure of bulk iron, the continued hydration, oxidation, hydroxidation, and oxy-hydroxidation process in Stage II lead to obvious structural and morphological changes in the top three atom layers of the bulk iron. The density of bulk material changes significantly in the concurrent chemical reactions of Stage II, in terms of the numbers of atoms contained in a unit volume. The penetration of oxygen atoms into the second or deeper layers leads to significant increase in the density of the bulk material. Instead of changing the crystalline structure of iron this process fills the lattice space in crystalline iron.

**Stage III:** Passivation of iron surface—as more water molecules become hydrated with iron surface, some Fe atoms in the oxides/hydroxides/oxy-hydroxides (generated originally from the top three layers of Fe atoms) start to separate from the bulk iron by losing all the metallic bonds from the surrounding Fe atoms. Such a metallic de-bonding mechanism leads to the generation of new bond between these Fe atoms and oxygen atoms in near vicinity. Therefore at the initial phase of State III, Fe atoms in the surface layers become more oxidized and most are bonded with more than one oxygen atoms. Some Fe atoms were observed to bond with more than three oxygen atoms to form a crystalline structure; however such crystalline structures only exist in small units and display an overall dis-ordered structure.

As a result of the continued oxidation, a triple-layered (or triplex) structure is formed gradually on top of the bulk iron sheet—an outer layer oxides/hydroxides/oxy-hydroxides with more oxygen atoms than Fe atoms owing to the sufficiency of atoms, an intermediate layer of oxides/hydroxides/oxy-hydroxides with approximately the same amount of oxygen atoms as Fe atoms, and an inner layers with more Fe atoms than the penetrating oxygen atoms. The intermediate layer of oxides/hydroxides/oxy-hydroxides and the inner Fe oxide layer both have a higher density than the outer layer. Within each of the three layers, however, there is no sign of a highly ordered crystalline structure being formed. Fig. 4 shows a snapshot of the triplex structure formed on steel surface in Stage III. It is noteworthy that due to the limited thickness of steel sheet modeled in Fig. 1, only one side of the nine-atom-thick sheet is exposed to bulk water to simulate the formation of triplex structure.

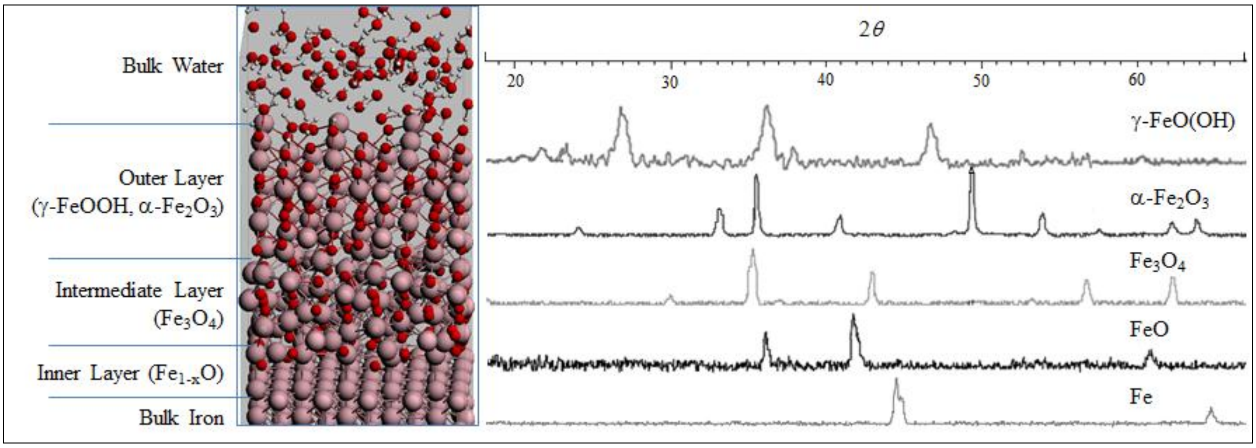


**Figure 4.** Atomistic Simulation Results vs. X-ray Diffraction (XRD) Spectra of Laboratory Samples

The overall hydration/oxidation/hydroxidation/oxy-hydroxidation of iron comes to equilibrium when the triple-layer structure is formed in State III. The chemical reactions after Stage III seem to be significantly slower than those in the previous phase/stages. These chemical reactions involve the penetration of oxygen atoms into the deeper layers beyond the third layer (as the forefront of the slow process), followed by continued oxidation/hydroxidation/oxy-hydroxidation of Fe atoms in the penetrated layers. The Fe oxides/hydroxides/oxy-hydroxides continue growing in the bulk iron until eventually all the metallic bonds are consumed. The snapshot in Fig. 5(a) shows the post-Stage III oxidation, and Fig. 5(b) gives the new chemicals generated. As oxidation/hydroxidation/oxy-hydroxidation of iron continues, individual Fe atoms become bonded with more oxygen atoms, leading to the destruction of the triplex structure and eventually a significant volumetric increase.

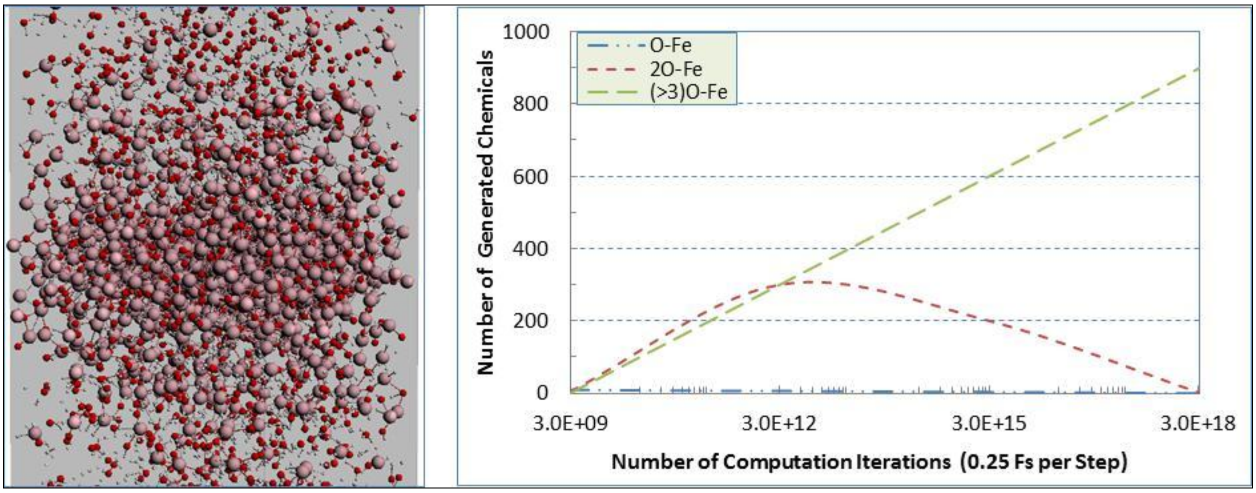


**Figure 5.** (a) Oxidation of Iron in Stage III; (b) Generation of New Chemicals in Stage III

The continued oxidation, hydroxidation and oxy-hydroxidation of iron atoms lead to the destruction of the crystalline structure of bulk iron and significant volumetric and morphological changes. Depending on the monitoring time and the new chemical products generated, the volume could increase by 6 times with significant density decrease.

### *2.1. X-ray Analyses and Model Validation*

The chemicals generated in Stages II and III were examined in this study using a hybrid method that involves the use of X-ray Reflectivity (XRR) to determine the in-situ thickness of the triplex sub-layers, and X-ray Powder Diffraction (XRD) to determine the chemical nature of the oxide/hydroxide/oxy-hydroxide materials. A low-carbon steel sample was allowed to corrode in deionized water (shown in Fig. 6 (a)) under the same ambient condition as the numerical simulation and subject to X-ray analysis at different stages.

The hybrid X-ray analyses were performed using a Philips X'Pert five-circle diffractometer. For the XRD measurements, the incident beam (Cu K$\alpha$ radiation with $\lambda$ = 1.5418 Å) was conditioned using a parabolic mirror to provide a high-intensity quasi-parallel beam. Tube power was set to 45 kV/40 mA to achieve a stable incident beam, and the detector ($2\theta$) axis was scanned from 15.0 to 90.0°. For the XRR measurements, the incident beam (Cu K$\alpha$ radiation with $\lambda$ = 1.5418 Å) was conditioned by a Soller slit assembly. Measurements were taken in a $\theta$–$2\theta$ geometry from $2\theta$ = 0.5° to $2\theta$ = 15.0° at the 30 kV/20 mA tube power to maintain linearity in the detector response.

According to the XRD spectra shown in Fig. 4, the oxidation products in the outer layer of the triplex structure are mainly hematite ($\alpha$-$Fe_2O_3$) surfaced with little amount of lepidocrocite [$\gamma$-$FeO(OH)$], the intermediate layer contains primarily magnetite ($Fe_3O_4$), and the inner layer is a wüstite ($Fe_{1-x}O$)-like material. The XRD results also agree well with the ReaxFF predicted chemical compositions of the triplex structure shown in Fig. 4.

$$n\lambda = 2d \cdot \sin\theta \tag{8}$$

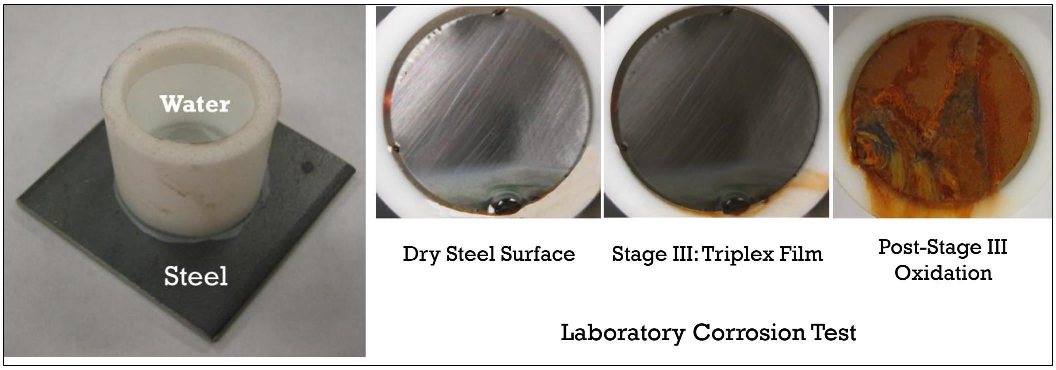


**A**

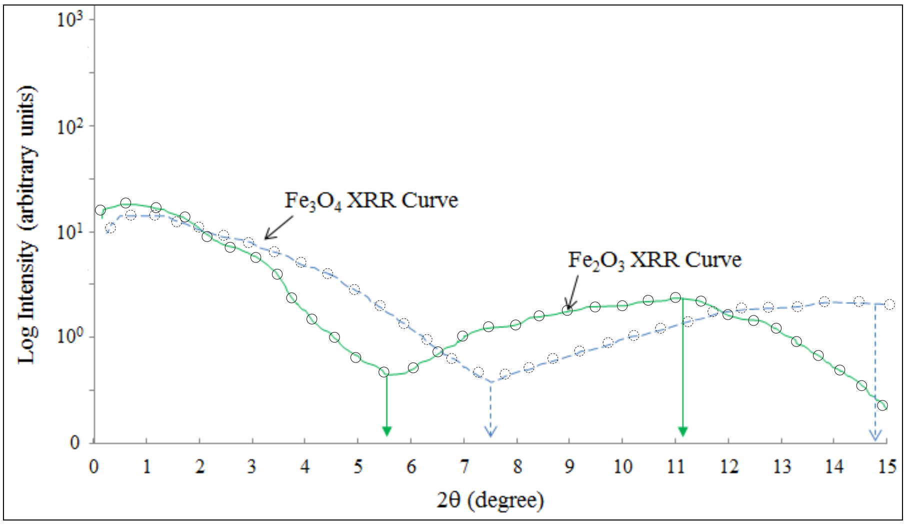


**B**

**Figure 6.** Laboratory Corrosion Test and XRR Results of the Triplex Structure (a)Laboratory Steel Oxidation/Corrosion Test(b) X-ray Reflectivity (XRR) Curves

The XRR results are shown in Fig. 6 (b). The fundamental framework for quantitative interpretation of XRR data was based on the pioneering recursion calculation by Parratt (*27*). Two different layers, one of hematite ($\alpha$-$Fe_2O_3$) and the other of magnetite ($Fe_3O_4$) was obtained in the Stage III oxidation. The thickness of the sub-layers in the triplex structure was determined using the

Bragg relationship given in Equation 8, where $n$ is the diffraction order, $\lambda$ is the wavelength of the incident X-rays, $d$ is the repeat unit thickness, $\theta$ *is* the angular position of the Bragg reflection. The thickness of the outer layer and intermediate layer were found to be equals 7.9 Å and t 6.0 Å, respectively. The XRR results were found to be in good agreement with the ReaxFF predicted thickness of the triplex sub-layers, with an outer layer = 7.8 Å and intermediate layer = 5.9 Å.

## 3. SUMMARY AND CONCLUSIONS

Active steel corrosion entails the formation and destruction of the passive film on steel surface. Central to the understanding of the two processes are the structure and dynamics of the oxidant/reductant atoms, ions and molecules in interaction with water molecules in the electric double layer. These two important steps however are highly thermodynamic in the sense that the speed and extent of corrosion significantly depends on the presence of chemicals and the toughness and thickness of the protective film. A clear picture of either step however is not available today, in term of the types and amount/thickness of the generated iron oxides, hydroxides and oxy-hydroxides, as limited by the experimental technologies available to plot one. This study was intended to visualize and accurately record the types and amount of new chemicals, and the morphological changes occurring in the formation of the passive film on steel surface using a combined QC simulation and X-ray based analyses. Conclusions based on this atomic study of rebar passivation in a typical concrete environment are summarized as follows:

1. The oxidation of individual iron atoms on steel surface is highly stochastic that is dependent on the thermodynamics and availability of oxygen atoms (from water molecules in this study);
2. The oxidation process of iron under the simulated condition (25°C and 1 ATM) involves a number of intermediate chemical species that do not exist as common iron minerals on earth, therefore can only be observed at the atomic-scale (due to the high chemical instability);
3. Early iron oxidation products are highly mixed and no phases were observed to consist of pure oxides/hydroxides/oxy-hydroxides seen on earth;
4. Three distinct stages of iron oxidation can be identified based on the composition and structure of the new chemical species generated in each stage, as well as the oxidation speed or how fast each stage is completed;
5. The high-chemical-stability triplex structure, after formed on steel surface, was observed to evolve at a significantly reduced speed, which tends to protect the bulk iron from further oxidation.

## References

1. D. L. Graver, *Corrosion Data Survey - Metals Section*, *Sixth Edition*, NACE. 1985.
2. C. C. Technologies, U.S. Federal Highway Administration (FHWA), Publication No. FHWA-RD-01-156, 2002.

3. H. G. Russell, NCHRP Synthesis 333, *Transportation Research Board, Washington, D.C.* 2004.
4. T. W. Neal, Jr, NCHRP Synthesis 257, *Transportation Research Board, Washington, D.C.* 1998.
5. R. J. Connor, R. Dexter, and H. Mahmoud, NCHRP Synthesis 354, *Transportation Research Board, Washington, D.C.* 2005.
6. W. H. Hartt, R. G. Powers, V. Leroux, and D. K. Lysogorski, U.S. Federal Highway Administration (FHWA), Publication No: FHWA-HRT-4-093, 2004.
7. D. A. Jones, *Principles and Prevention of Corrosion (2nd Edition)*, Prentice Hall, Upper Saddle River NJ, 1996.
8. L. L. Shreir, R. A. Jarman, and G. T. Burstein, *Corrosion*, Butterworth-Heinemann, Oxford, Boston, 1994.
9. J. Kruger, *International Materials Reviews*, 33. 1988.
10. T. Pan, T. Nguyen, and X. Shi, *Journal of the Transportation Research Board–Transportation Research Record (TRR): No.* 2044, National Research Council, Washington, D.C.. 2008.
11. T. Pan, and L. Wang, *ASCE Journal of Engineering Mechanics.* Vol. 137, No. 5. 2011.
12. S. Nesic, Corros. Sci. 49, 4308-4338. 2007.
13. C. Noubactep, *Water SA*, ISSN: 0378-4738, 36 (5), 663-670. 2010.
14. P. G. Tratneyk, Putting corrosion to use: Remediating contaminated groundwater with zero-valent metals. *Chem. Ind*. 1996.
15. H. H. Uhlig, J. Electrochem. Soc., Volume 115, Issue 4, pp. 108C-111C. 1968.
16. H. H. Strehblow, *Materials and Corrosion*, Volume 35, Issue 10, pages 437–448, 1984.
17. H. W Song, and V. Saraswathy, *Int. J. Electrochem. Sci.*, 2, pp.1- 28. 2007.
18. C. M. Hansson, A. Poursaee, and S. J. Jaffer, *PCA R&D Serial No. 3013*, Portland Cement Association, Skokle, Illinois, USA. 2007.
19. R. M. Cornell, and U. Schwertman, *The Iron Oxides: Structure, Properties, Reactions, Occurrences and Uses*. Wiley-VCH, ISBN: 3-527-30274-3. 2003
20. E. Herzberg, *DoD Updates Report on Cost of Corrosion for Marine Corps Ground Vehicles*. Volume 6, No. 2, 2010.
21. R. G. Parr, and W. Yang, *Density-Functional Theory of Atoms and Molecules*. New York: Oxford University Press. ISBN 0-19-504279-4. 1989.
22. A.C.T. van Duin, S. Dasgupta, F. Lorant and W.A. Goddard, *J. Phys. Chem. A*, 105. 2001.
23. M. Aryanpour, A. C. T. van Duin, and J. D. Kubicki, *J. Phys. Chem. A,* 114. 2010.
24. W.J. Mortier, S.K. Ghosh, and S. Shankar, *J. Am. Chem. Soc.* 108, 4315. 1986.
25. G.O.A. Janssens, B.G. Baekelandt, H. Toufar, W.J. Mortier, and R.A. Schoonheydt, *J. Phys. Chem.* 99, 3251. 1995.
26. S.L. Njo, J. Fan, van de Graaf, B. *J. Mol. Catal. A* 134, 79. 1998.
27. L.G. Parratt, *Phys. Rev.* 95, pp. 359-369. 1954.